JOURNAL OF AIRCRAFT
Vol. 49, No. 2, March–April 2012

Simulation of Supercooled Large Droplet Impingement via Reduced Order Technology

Marco Fossati* and Wagdi G. Habashi†
McGill University, Montreal, Quebec H3A 2S6, Canada
and
Guido S. Baruzzi‡
Newmerical Technologies International, Montreal, Quebec H3A 2M7, Canada

DOI: 10.2514/1.C031608

The computational cost of viscous turbulent aeroicing simulations is a limitation that needs to be addressed more extensively using computational fluid dynamics (CFD) for aircraft in-flight icing certification. To overcome this computational burden, a reduced-order modeling (ROM) approach, based on proper orthogonal decomposition and kriging interpolation techniques, is applied to the computation of the water impact pattern of supercooled large droplets on aircraft. Relying on an appropriate database of high-fidelity, full-order simulations, the ROM approach provides an accurate lower-order approximation of the system in terms of a linear combination of appropriate functions. The resulting surrogate solution is successfully compared with experimental and CFD results for two-dimensional and three-dimensional cases, including a complete aircraft case.

I. Introduction

AIRCRAFT flying through clouds of supercooled liquid droplets (SLD) can be subjected to in-flight ice accretion. Surface tension prevents the expansion of the droplets that would occur with phase change, forcing them to remain in liquid form even though their temperature is below the freezing point. When the droplets hit an aircraft's surfaces, the surface tension decreases at the contact point, and they may freeze completely on impact if the temperature is very low or freeze partially at higher temperatures, whereas the remaining liquid portion runs back on the surface, transported by the pressure gradient and the shear stress of the airflow. If no ice protection is provided, the aerodynamic characteristics of the aircraft and its handling can be severely degraded when ice accretes. The increased drag generated by the roughness of the ice can lead to flow separation, reduction of the stall margins, control reversals, and engine blockages [1].

Airworthiness of transport airplanes in icing conditions is demonstrated by compliance with certification standards (Appendix C of the FAA Federal Aviation Regulations, part 25) set by agencies, such as the Federal Aviation Administration, European Air Safety Association, Transport Canada, etc. These standards, frozen for 50 years, will soon undergo significant revisions with the adoption of Appendix O to address the icing threat posed by SLD conditions. Unlike smaller droplets, SLD can distort, break into smaller droplets, splash, bounce off surfaces, get carried downstream by the flow, and reimpinge, increasing the potential for ice contamination on unprotected surfaces [2–4]. Nowadays, wind tunnel tests, icing tunnel tests, and computer simulations play major complementary roles in the process of certifying a new aircraft [5,6]. Advances in modeling capabilities have created the conditions to accurately simulate the ice accretion process in a realistic three-dimensional (3-D) context [7,8]. Unfortunately, the computational cost associated with performing a multitude of 3-D simulations of various aeroicing conditions somewhat limits the widespread use of computational fluid dynamics (CFD), even if advanced computational resources are available [9,10]. To overcome this difficulty, mostly low-cost and, consequently, low-fidelity tools are usually employed. These may be based on empirical correlations, two-dimensional (2-D) approximations, inviscid or incompressible flow assumptions, and/or other simplifications that result in limited accuracy and realism.

A viable alternative is the reduced-order modeling (ROM) approach [11,12], which dramatically reduces the cost of high-fidelity simulations while providing solutions of superior accuracy to low-fidelity methods because it preserves the detailed physical modeling of the problem under consideration [13–16]. Although the use of this approach in the aeroicing environment is in its pioneering phase, recent results support the effectiveness of this methodology as a valuable tool in the context of a multicondition, multiparameter certification process [17–20].

In a framework of ice accretion simulation as the succession of airflow, water concentration, and heat transfer calculations, the most time-consuming part is obtaining the water impact patterns. The common practice is to assume a distribution of discrete droplet diameters, compute the impingement distribution of each diameter class, and weight-average these monodispersed solutions. In the case of the droplet sizes of Appendix C, seven distinct monodispersed sizes (Langmuir-D distribution) are used to compute the overall impingement distribution. In the SLD regime, however, due to the complex phenomena of droplet breakup, splashing, and bouncing, distributions containing up to 27 diameters of monodispersed droplets are needed to obtain realistic impingement predictions [5–7]. The computational cost of an SLD simulation is hence four times that of a Langmuir-D distribution. In the present work, it will be shown that the ROM approach can dramatically reduce cost with only a very modest degradation of the overall accuracy of the simulation.

The essentials of the ROM approach used to extract the solution eigenfunctions (or modes) and compute solutions at unknown states are introduced in sections II and III of this paper, whereas section IV illustrates the interpolation technique used to compute the surrogate solutions. Finally, 2- and 3-D results and comparison with experiments and other methods are presented to validate the present methodology.

Received 29 July 2011; revision received 14 September 2011; accepted for publication 15 September 2011.

*Postdoctoral Research Associate, Mechanical Engineering, Computational Fluid Dynamics Laboratory, 688 Sherbrooke Street West; mfossati@cfdlab.mcgill.ca. Member AIAA (Corresponding Author).

†Professor and Director, NSERC-J. Armand Bombardier-Bell Helicopter-CAE Industrial Research Chair of Multidisciplinary Computational Fluid Dynamics Laboratory, Department of Mechanical Engineering, 688 Sherbrooke Street West, Fellow AIAA.

‡Research & Development Director, 688 Sherbrooke Street West, Member AIAA.

II. Reduced-Order Modeling

The main goal of a ROM approach is to lower computational cost while maintaining accuracy close the high-fidelity model. This is achieved through complex mathematical techniques that, given a set of initial high-fidelity observations of the system, isolate the inmost relevant features in terms of a limited number of orthogonal functions and subsequently use these extracted modes to reformulate the dynamics of the system in a computationally more tractable way [21,22]. In fact, given a set of orthogonal basis functions, it is possible to project the original system of equations onto the space spanned by these functions and to obtain an equivalent reduced system. The solution of the reduced system would have by then inherited the computational complexity of the few dozens degrees of freedom that are left by the projection operation, rather than the tens of millions typical of aerospace applications [23,24]. The key elements of this process are as follows: 1) the selection of the observations (snapshots) of the system, 2) the extraction of the dominant features into a finite set of functions, and 3) the solution of the reduced system.

Following the methodology reported in the recent literature in the context of aeroicing via ROM [17–19], the actual solution of the reduced system is not computed explicitly; only the surrogate solution for any arbitrary initial/boundary condition is obtained directly as a linear combination of the extracted modes. In this way, the solution of the reduced system is replaced by the computation of a few dozen scalar coefficients, i.e., as few as the extracted modes. This shortcut is made possible by the adoption of the well-known proper orthogonal decomposition (POD) technique [13,14]. Postponing the mathematical details to the next section, the rationale for this is that because any state of the system can be represented as a linear combination of modes, snapshots obtained via high-fidelity computations provide the information to determine the scalar coefficients by which other snapshots can be reconstructed as a sum of basis functions. Pairing these known scalar coefficients and the initial/boundary conditions of the snapshots, it is possible with standard interpolation techniques to obtain the unknown coefficients for any new set of initial/boundary conditions.

III. Proper Orthogonal Decomposition

The POD, also known as singular value decomposition or Karhunen-Loëve decomposition, is a method in the field of principal component analysis that is used to extract and combine appropriate eigenfunctions (also called modes) to represent complex spatial-temporal fields [13,14]. Although it is a linear procedure, in the sense that solutions are obtained in terms of a linear combination of functions, this technique is still able to reproduce many of the nonlinear features of the system under examination. This approach can then be applied to complex nonlinear simulations, such as fluid flows [25,26].

To calculate the modes from the computed snapshots, consider an ensemble of N_S snapshots of the system indicated as $\vec{U}$ in $\mathbb{R}^{N_P}$, where N_P is the number of grid points. The objective is to find a basis vector for the ensemble of data such that a finite-dimensional representation of the form

$$\vec{U} = \sum_{i=1}^{N_S} \alpha_i \vec{\phi}_l \tag{1}$$

with α_i in $\mathbb{R}$ and $\vec{\phi}$ in $\mathbb{R}^{N_P}$ represents any member of the ensemble better than any other linear representation of the same dimension using any other basis function in a least-squares sense. The optimal basis can be computed by resorting to the method of snapshots introduced by Sirovich [26]. The first step is to define the correlation matrix of the snapshots, R, which defines how each snapshot is related to the others in terms of the scalar products of snapshots:

$$R_{ij} = \frac{1}{N_S}(\vec{U}_i, \vec{U}_j) \tag{2}$$

The second step is to solve the eigenproblem $R\vec{\beta} = \lambda\vec{\beta}$ that results from the error-minimization condition [18]. Once the eigenvectors of the system are obtained, the desired eigenfunctions can be computed as follows:

$$\vec{\phi}_l = \sum_{j=1}^{N_S} \vec{\beta}_j^l \vec{U}_j \qquad i = 1, \ldots, N_S \tag{3}$$

The basis functions $\vec{\phi}_l$ span a vector space Φ that contains all possible states of the dynamical system described by the snapshots. This means that a particular solution of this system can be obtained as a linear combination of modes. In other words, given an arbitrary set of initial/boundary conditions, the corresponding solution, $\vec{V}$, can be written as

$$\vec{V} = \sum_{i=1}^{N_S} \tilde{\alpha}_i \vec{\phi} \tag{4}$$

where the suitable N_S coefficients, $\tilde{\alpha}_i$, have to be computed. For this purpose, let us recall that, by knowing the snapshots $\vec{U}_l$ and the modes $\vec{\phi}_l$, the snapshot-related $\vec{\alpha} = \{\alpha_1, \alpha_2, \ldots, \alpha_{N_s}\}$ can be obtained by inverting Eq. (1), i.e.,

$$\alpha_i = (\vec{U}_l \vec{\phi}_l) \qquad i = 1, \ldots, N_S \tag{5}$$

Equation (5) implicitly defines a correspondence between the snapshots and, in turn, the relative initial/boundary conditions, and this relation can be exploited to compute the missing $\tilde{\alpha}_i$ in Eq. (4) using interpolation techniques, as outlined in the next section.

IV. Kriging Interpolation Technique

The N_S snapshot-related pairs (initial/boundary condition, $\vec{\alpha}$) define the N_S hypersurfaces $\alpha(\vec{x})$, defined in $\mathbb{R}^{N_V}$, and with values in $\mathbb{R}$. Here, the shortcut $\vec{x}$ has been used to indicate a specific set of initial/boundary conditions for the problem, whereas N_V is the number of free parameters. The problem of finding $\tilde{\alpha}(\vec{x})$ can then be recast as a problem of multidimensional interpolation along these hypersurfaces. In most of the parametric applications of the ROM approach, a polynomial interpolation is used to determine the coefficients, and in this work, the so-called ordinary kriging interpolation method has been adopted [27–29]. Kriging is chosen here in preference to Akima [19], as it accepts an arbitrary number of design variables with no impact on the computational cost of the interpolation phase or on the accuracy of the interpolated solution. Although this choice might not appear necessary here, as only one design parameter is considered, the intent is to develop an algorithm, general in nature with no limit as to dimensionality, as future investigations may require the adoption of additional parameters, for which interpolation techniques might not work as efficiently as in kriging [28].

The mathematical details of the method are as follows. Consider the problem of computing the *i*th coefficient corresponding to the *i*th mode. The ordinary kriging technique provides the following formula:

$$\tilde{\alpha}_i(\vec{x}) = \gamma + Z\vec{x} \tag{6}$$

where γ is a constant global model, and Z is a perturbation over the global model given by

$$Z(\vec{x}) = \vec{\gamma}^T M^{-1}(\alpha_i - \vec{\mathbf{1}}_\gamma) \tag{7}$$

where $\mathbf{1}$ is a unit vector introduced for dimensional agreement. The matrix $\mathbf{M}$ and the correlation vector $\vec{r}(\vec{x})$ are obtained as follows:

$$M(\vec{x}_i, \vec{x}_j) = \mathbf{exp}[-\sum_{k=1}^{N_V} \theta_k |x_k^i - x_k^j|^2] \qquad i, j = 1, \ldots, N_S \tag{8}$$

$$\vec{r}(\vec{x}) = \{M(\vec{x}, \vec{x}_1), \ldots, M(\vec{x}, \vec{x}_{N_S})\} \tag{9}$$

In other words, the matrix **M** defines a distance in a statistical sense between the initial/boundary conditions of the snapshots, whereas the vector $\tilde{r}(\vec{x})$ is constructed by evaluating the same distance function between the target value and each snapshot. The global model γ is eventually computed as follows:

$$\gamma = \frac{\vec{1}^T M^{-1} \vec{\alpha}}{\vec{1}^T M^{-1} \vec{1}} \tag{10}$$

The only unknowns to be estimated are the N_V scalar values of the weight θ_k. These parameters can be estimated by maximizing the likelihood function [28,29]:

$$Ln = -\frac{1}{2}[N_S \ln(\sigma^2) + \ln |M|] \tag{11}$$

where $\sigma^2 = 1/N_S(\vec{\alpha} - \vec{1}_\gamma)^T M^{-1}(\vec{\alpha} - \vec{1}_\gamma)$. In the present algorithm, the maximization is performed using genetic algorithms, and the values of θ_k that lead to the maximum of the likelihood function are selected. The parameters θ_k act as weights that define distances between the sample points and how the samples are correlated.

V. Validation of the CFD Methodology

The computation of the droplet impingement distribution is a fundamental prerequisite in the simulation of in-flight ice accretion because it determines the extent and quantity of water accumulation on the aircraft surfaces. Two important parameters that affect the impingement distribution are the droplet median volumetric diameter (MVD) and the cloud liquid water content (LWC). The latter provides a measure of the density of water droplets in the cloud, and the former is the average size of the droplets dispersed in the cloud. Droplets dispersed in clouds exhibit a range of diameters; therefore, a variety of diameter distributions can be adopted to describe the composition of the cloud for a particular MVD. These distributions represent the cloud composition in terms of percent LWC content for a discrete set of diameters.

2-D droplet impingement results are presented in this section to validate the methodology adopted for the full-order SLD simulations against available experimental data. The high-fidelity CFD solutions are obtained through DROP3D, the water impingement module of the FENSAP-ICE simulation system. DROP3D is based on a Eulerian approach [9] where conservation equations for mass and momentum of the water-fraction are solved simultaneously in a finite element framework. The treatment of SLD conditions by Honsek et al. [7] relies on the theory of Pilch and Erdman [30] for modeling the breakup phenomena, whereas the effects of splashing and bouncing are modeled by the approach of Trujillo et al. [31]. The computational approach adopted by DROP3D is such that, for each droplet distribution (Langmuir or any other type of user-defined distribution) centered on a given MVD, a discrete set of N droplet diameters are defined and used to perform N independent monodispersed simulations. The effects of breakup, splashing, and bouncing are taken into account automatically for droplet diameters in the SLD range. The monodispersed solutions are then weight-averaged to provide the cumulative impingement distribution associated with the given MVD.

VI. Supercooled Large Droplet Impingement on a NACA23012 Airfoil

This section presents data to compare the full-order methodology for the simulation of droplet impingement with available experimental results. The experimental data is contained in the reference work for SLD cases by Papadakis et al. [5]. Among the different icing conditions they considered, two specific SLD cases have been chosen for the computational analysis, the first one where MVD = 111 μm and the second one where MVD = 236 μm. Two geometries have been considered: the classical National Advisory Committee for Aeronautics (NACA) 23012 airfoil and the NACA 23012 airfoil with leading-edge double-horn glaze ice contamination after 45 min. exposure, as obtained by the NASA code LEWICE. A structured grid made of 53,504 hexahedral elements and 108,208 nodes is generated for the clean configuration. A hybrid grid is instead adopted for the contaminated airfoil containing 149,751 nodes, 119,033 hexahedral elements, and 59,991 prismatic elements. The latter is the result of two levels of adaptation with a mesh optimization algorithm driven by the flow solution [32]. The details of the impingement calculation are: LWC = 0.73 g/m^3 with a 27-diameter droplet distribution as indicated in Table 1 for the case of MVD = 111 μm, and a case in which LWC = 1.89 g/m^3 and a 27-diameter droplet distribution for the case of MVD = 236 μm is indicated in the same Table 1. The flow conditions are: Mach number = 0.2287, Reynolds number = 4.56×10^6, and angle of attack = 2.5°. Figure 1 shows the LWC contours and collection efficiency, β, for MVD = 111 μm obtained with DROP3D. Figure 2 illustrates the same comparison in the case of MVD = 236 μm. The agreement of the computed distributions with the experimental results is satisfactory.

The contaminated NACA 23012 airfoil is a more challenging test than the clean one, as the irregular shape of the surface increases the complexity of breakup, bouncing, and splashing effects. Figures 3 and 4 show the LWC contours and the comparison of the β distributions compared with the experimental results for the two different MVDs. The results obtained by LEWICE and the one presented by Papadakis et al. [5] are also included.

VII. 2-D Numerical Tests via Reduced-Order Modeling

The ROM technique is now applied to the previous four 2-D test cases to assess its accuracy in reproducing the full-order results while reducing the computational cost. For this purpose, the droplet

Table 1 Twenty-seven-diameter distributions from Papadakis et al. [5]

Bin	MVD = 111 μm	MVD = 236 μm	% LWC	Bin	MVD = 111 μm	MVD = 236 μm	% LWC
1	10.87	15.91	4.75	15	152.83	455.54	4.75
2	24.52	45.34	4.75	16	165.86	494.62	4.75
3	29.64	74.84	4.75	17	179.36	534.11	4.75
4	34.96	102.04	4.75	18	193.73	577.96	4.75
5	44.74	122.55	4.75	19	207.19	624.02	4.75
6	58.63	141.63	4.75	20	219.68	670.92	4.75
7	70.67	160.54	4.75	21	2279	701.15	1.00
8	81.29	178.45	4.75	22	230.14	713.63	1.00
9	91.19	197.69	4.75	23	237.75	728.34	1.00
10	100.94	217.96	4.75	24	250.52	742.11	0.50
11	110.60	240.80	4.75	25	264.23	752.68	0.50
12	119.49	271.02	4.75	26	279.54	763.25	0.50
13	128.83	320.0.	4.75	27	312.59	1046.77	0.50
14	140.11	393.53	4.75				

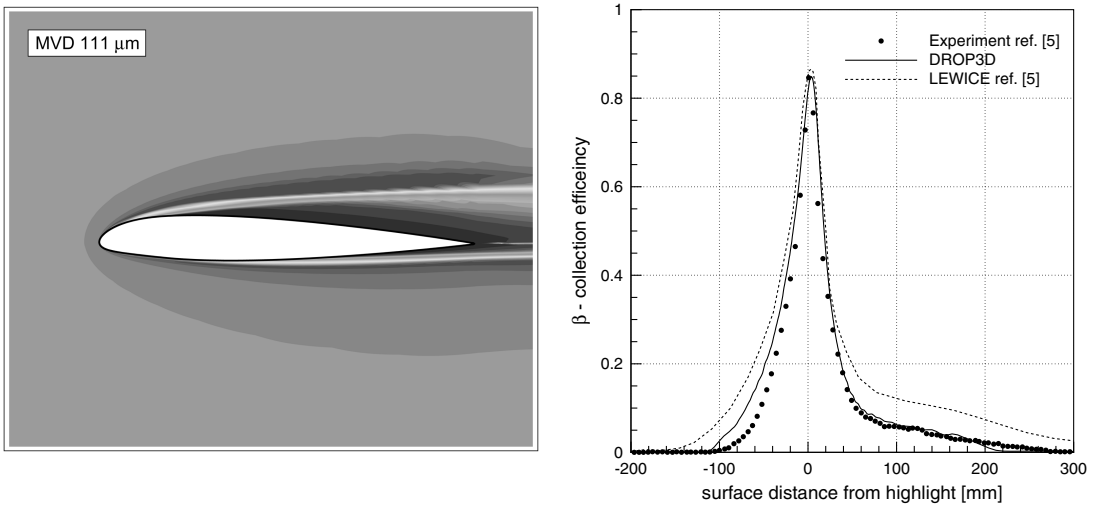

Fig. 1 MVD = 111 μm: LWC contours (left) and collection efficiency (right).

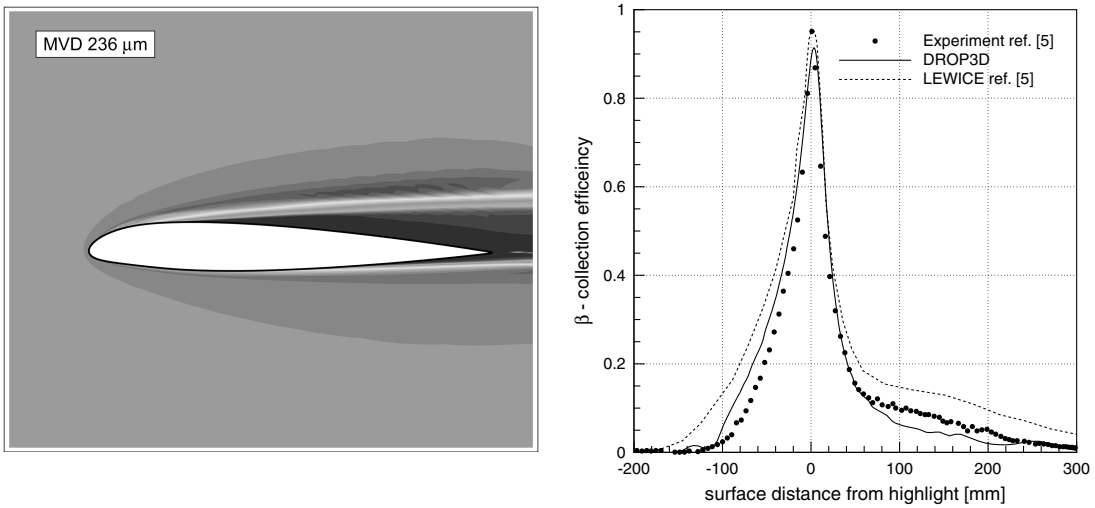

Fig. 2 MVD = 236 μm: LWC contours (left) and collection efficiency (right).

diameter is the only free parameter considered (i.e., $N_V = 1$) by which a suitable number $N_S < 27$ of monodispersed solutions are selected and used to extract the basis functions. The α-hypersurfaces in these specific cases are 2-D curves in the plane diameter-α. Kriging interpolation, together with the POD-based linear combination, are used to obtain the monodispersed solutions corresponding to the missing 27-N_S diameters. The same weighted averaging procedure used in the full-order approach is used to obtain the combined effect of all the diameters, according to the LWC distribution of Table 1. Similar results have been recently published in the literature by the

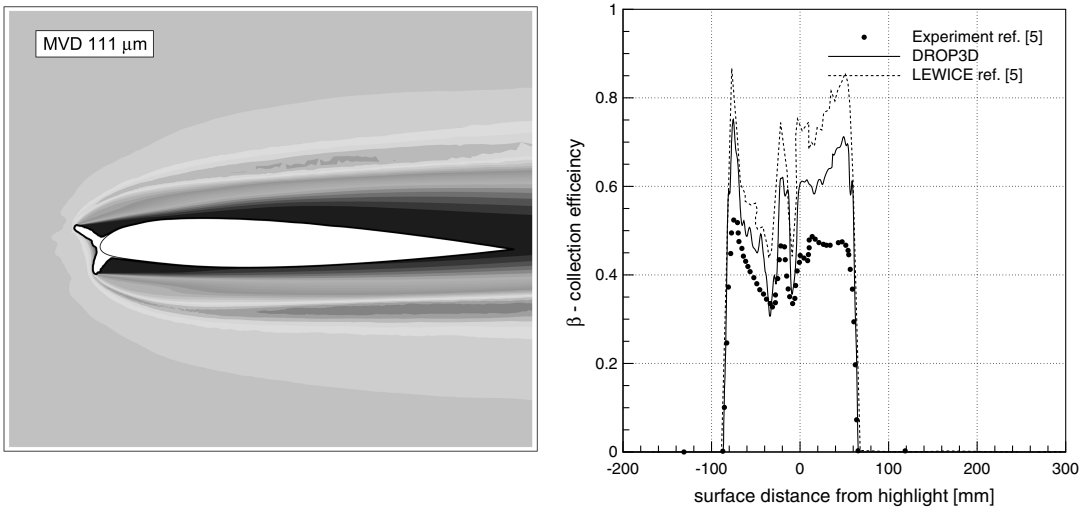

Fig. 3 MVD = 111 μm: LWC contours (left) and collection efficiency (right).

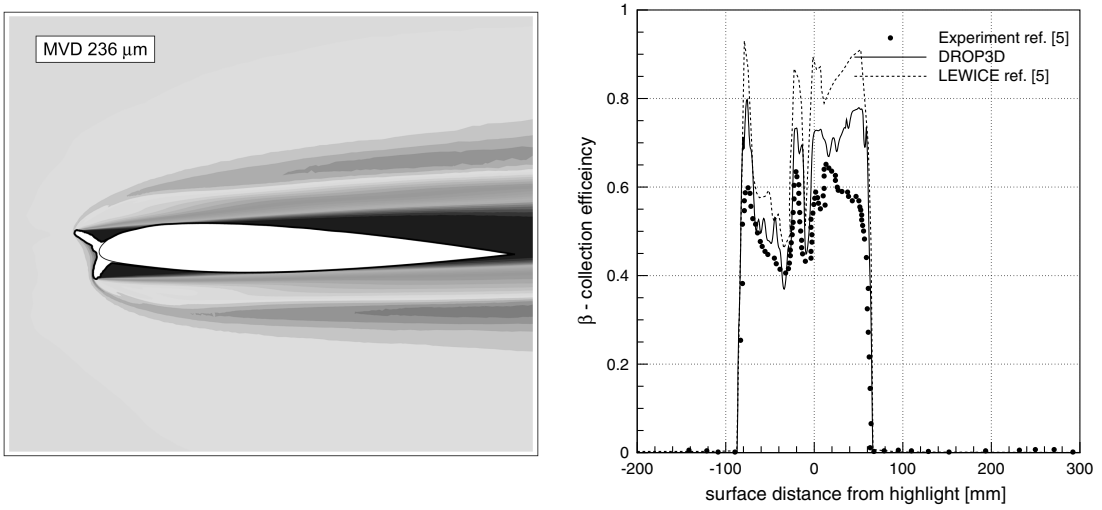

Fig. 4 MVD = 236 μm: LWC contours (left) and collection efficiency (right).

present authors [17]; however, the current study introduces new results and a more detailed analysis of the convergence of the ROM solutions to the full-order results.

A fundamental problem in ROM is the selection of the optimal set of snapshots, both in terms of the number and value of the free parameters. In fact, to the best of the authors' knowledge, there is no consistent or generally accepted methodology capable of selecting the optimal snapshots that yield the best surrogate model as a trade-off between the computational cost of obtaining the snapshots and the accuracy of the resulting reduced-order solution. In this work, a heuristic approach is presented, in which the results of several combinations of a different number of snapshots have been tested and proven to be satisfactory in terms of specified accuracy with respect to the full-order solutions. It is not possible to test all of the configurations of snapshots, as if one assumes that among the entire set of 27 solutions, three snapshots corresponding to the smallest, the biggest, and the MVD diameters are always selected, one is left with the selection of a specific set of N_S among the remaining 24 solutions, where both N_S and the specific values are unknown. By combinatorial analysis, it can be shown that for this SLD investigation one would have to evaluate up to 17×10^6 different combinations! Clearly, this is impractical and beyond the scope of the present work, whose focus is on the application of the surrogate modeling approach to the cost reduction of SLD impingement calculations. The heuristic approach for the snapshots is thus to first select the snapshots with higher values of LWC, trying to sample uniformly the range of diameters considered. The selection procedure is eventually stopped when the set of snapshots is able to provide an accuracy of 10% in β and an accuracy of 2% in water catch in kg/s, with respect to the full-order solution. The difference in magnitudes of the two thresholds is because the water catch is an integrated quantity, as opposed to β, which is a local quantity, on the surface.

The sensitivity of the surrogate solution with respect to the selected snapshots has not been thoroughly investigated due to the impossibility of analyzing millions of combinations, but only by checking a couple of different selections. The results have shown that, for SLD impingement problems, no significant difference is observed. That is the reason why the results presented here can be considered somewhat conclusive, despite the empiricism adopted in the selection of the snapshots. The concept of error threshold as a stop criterion in the snapshots selection would require the knowledge of the full-order solution, which is what we want to avoid computing, and hence cannot be applied in general usage. Nevertheless, this preliminary analysis can be helpful to gain expertise in formulating a priori empirical estimates of the optimal set of snapshots.

The 2-D results obtained via the present ROM approach for the NACA 23012 cases are shown in Figs 5–12. They are the collection efficiency, the convergence curves for the L_2 norm of the error in β, the water catch, and the bar plots of the LWC distributions. Figures 5–8 show the results of the heuristic procedure for the clean airfoil. It can be shown that, for the two MVD cases, as few as nine snapshots are sufficient to provide collection efficiency distributions that agree very well with the full-order solution. The pictures also show that the β distribution obtained using 21 snapshots has an error lower than 1% and that it almost coincides with the full-order 27-diameter solution. In this case, with nine snapshots, the error in β is 3.5% in the case of 111 μm and 2.7% in the case of 236 μm. The error in water catch is slightly less than 2% for the 111 μm case and 0.46% for the 236 μm case.

Figures 9–12 illustrate the same trends in the case of the ice-contaminated airfoil. Because of the higher complexity of this test, the number of snapshots that guarantees an L_2 norm of the error in β smaller than 10% is 11 and 13 for the case at 111 μm and 236 μm, respectively. Also, in this case, a surrogate solution obtained with 21 snapshots that shows negligible (i.e., <1%) difference with respect to the 27-diameter solution is reported for comparison. The error in β is 8.6% for the 111 μm case and 9.3% for the 236 μm case, whereas the error in water catch is 0.8% for the 111 μm case and 1.3% for the 236 μm case.

To verify the importance of including the surrogate solutions, Figs. 9 and 11 present β and water catch obtained by simply combining the selected snapshots (postfix average) and compare them to results using the snapshots + surrogate solutions. The figures clearly show that the addition of the surrogate solutions to the set of snapshots is necessary, as it captures many fundamental features.

Typically, the computational time required by a ROM solution is of the order of a fraction of a second. Thus, the evaluation of the savings in central processing unit (CPU) time can be regarded as simply the ratio between the time required to compute the number of adopted snapshots vs the time required to compute the reference 27 solutions of DROP3D. This means that, in the case of the clean airfoil at the two different MVDs, the saving in time is twothirds, or conversely, the present ROM approach provides reasonably accurate solutions in onethird of the time of a full-order approach. In the case of the ice-contaminated airfoil, good solutions are obtained in slightly less than one-half of the time of the full-order solution.

VIII. 3-D Impingement via Reduced-Order Modeling

The true power of the ROM approach is revealed when realistic 3-D problems are analyzed. In this section, the computation of the impingement distribution over the surfaces of an aircraft is considered. The geometry is the DLR-F6 fuselage, wing, pylon, and nacelle. The computation of the collection efficiency for this type of problem is very important from an engineering point of view because it takes into account not only the droplet impingement along the

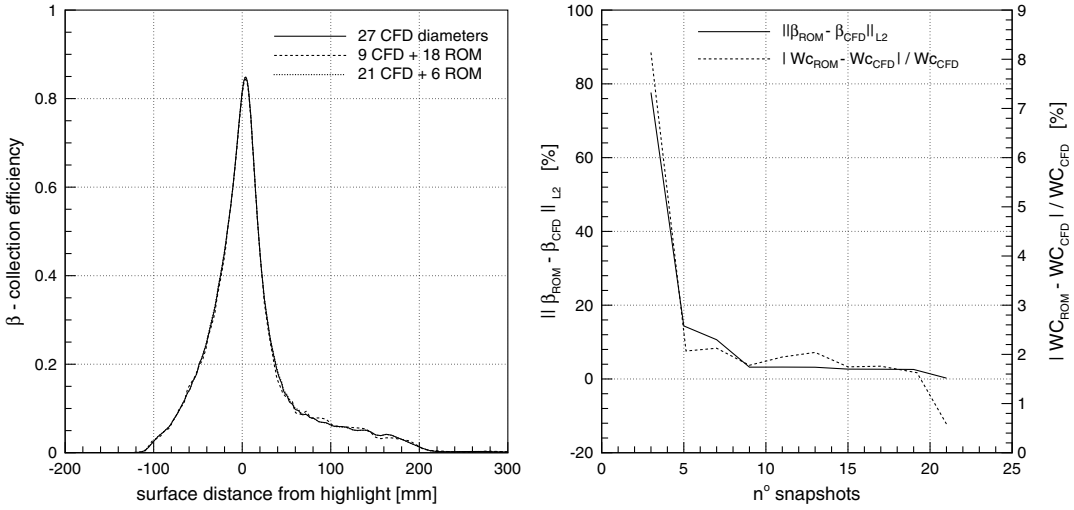

Fig. 5 MVD = 111 μm: Collection efficiency (left) and error convergence with regard to full-order 27-diameter solution, WC = water catch, kg/s (right).

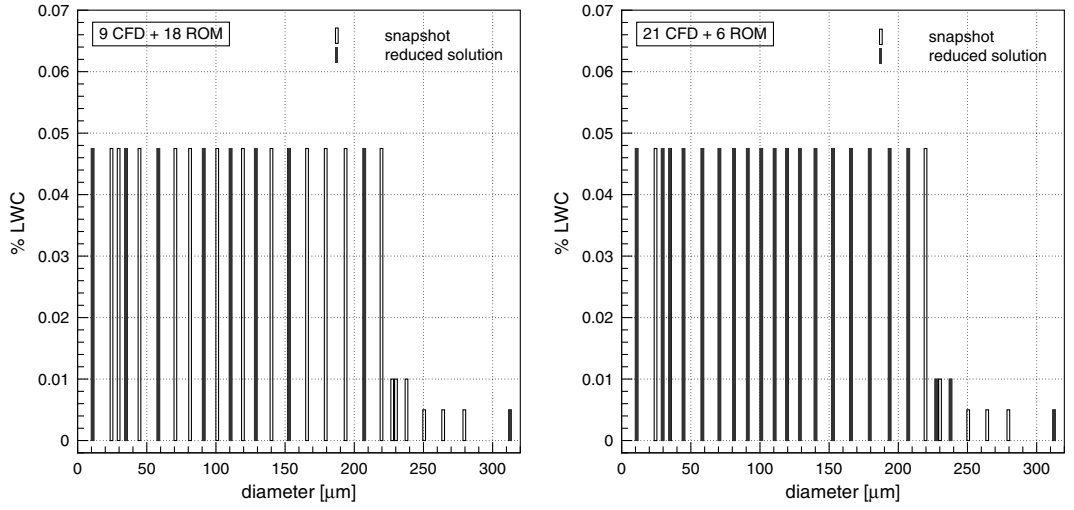

Fig. 6 Snapshots for the noncontaminated NACA23012 at 111 μm: nine-solution set (left) and 21-solution set (right).

leading edge of the wing but also on the engine nacelle, which is a critical component that must be protected from icing. Note that the solutions presented here consider the full interaction between components and are not obtained from 2-D cross-sectional cuts. A hybrid grid containing of 2,281,111 nodes, 3,823,680 prismatic elements, and 1,875,932 tetra elements is employed for the simulations. The airflow conditions are typical of a holding pattern, i.e., Mach number = 0.3, Reynolds number = 3.5386×10^6, and

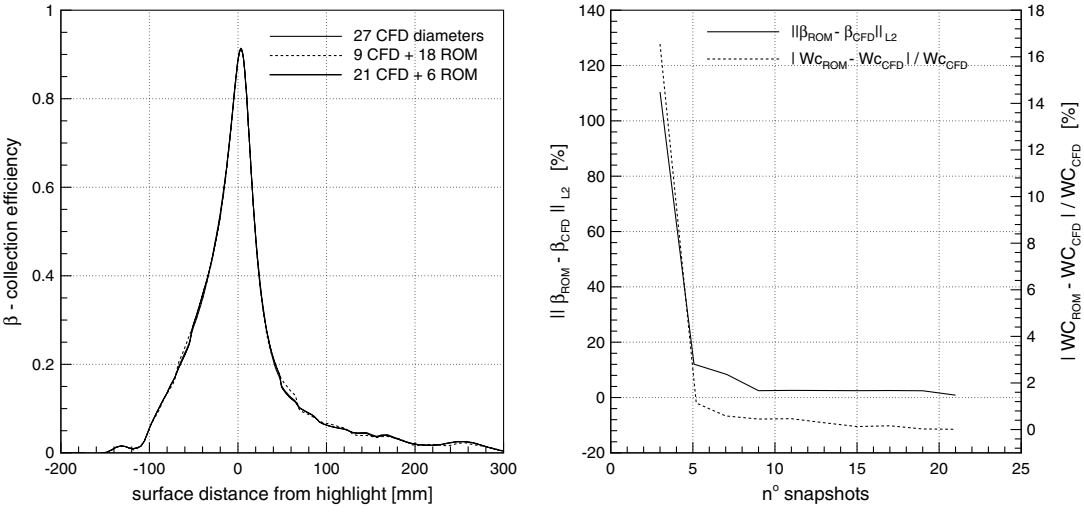

Fig. 7 MVD = 236 μm: Collection efficiency (left) and convergence with regard to the 27-diameter solution, WC = water catch, kg/s (right).

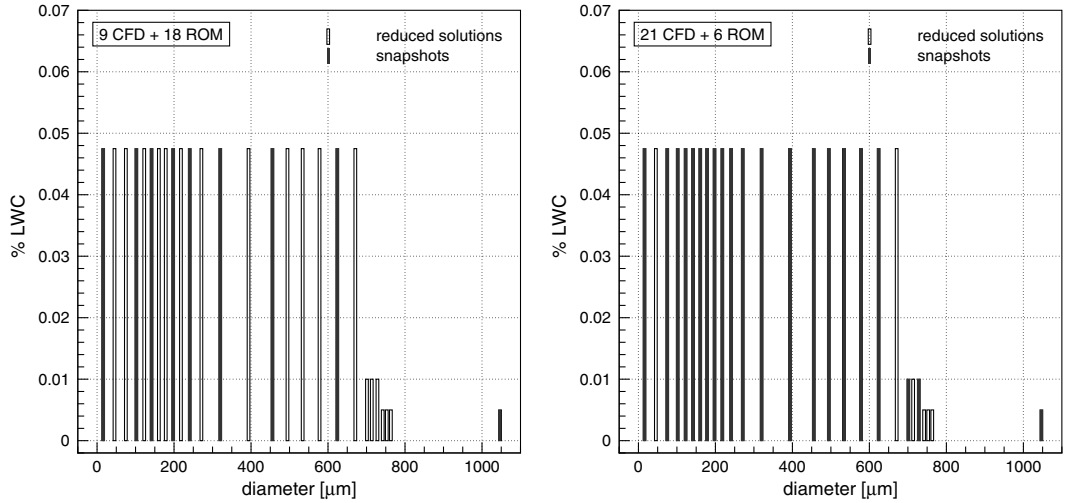

Fig. 8 Snapshots for the noncontaminated NACA23012 at 236 μm: nine-solution set (left) and 21-solution set (right).

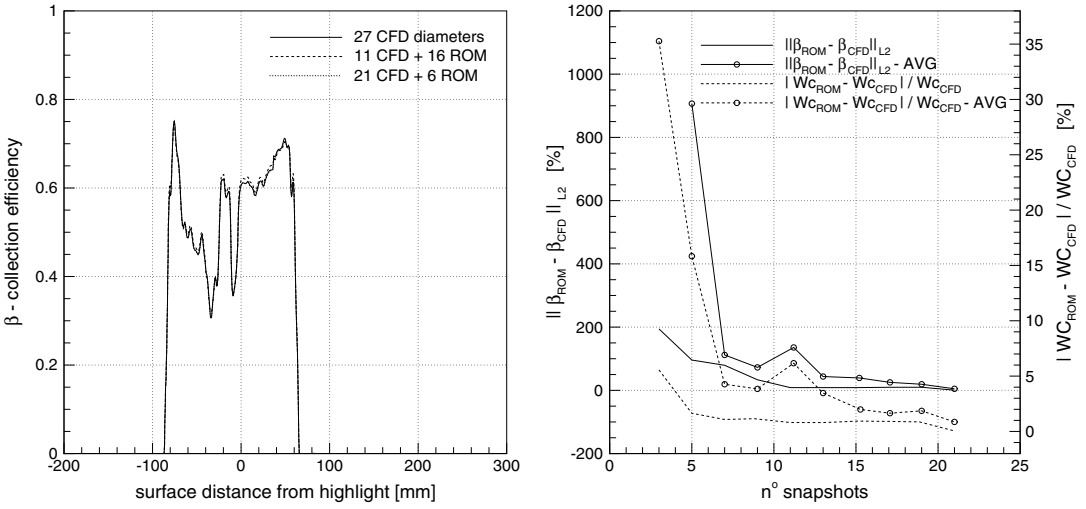

Fig. 9 MVD = 111 μm: Collection efficiency (left) and error convergence with regard to full-order 27-diameter solution, WC = water catch, kg/s (right).

angle of attack = 2.5°. In this case, the droplet impingement has been computed only on the clean configuration, assuming an MVD= 236 μm, a LWC = 1.89 g/m^3, and with a 27-diameter pseudo-Langmuir distribution. The latter has been chosen because this type of distribution closely represents the actual droplet distribution in the clouds. It has been obtained via interpolation from a sample 10-diameter distribution reported by Papadakis et al. [5]. Table 2 illustrates the adopted LWC-diameter distribution. The left part of

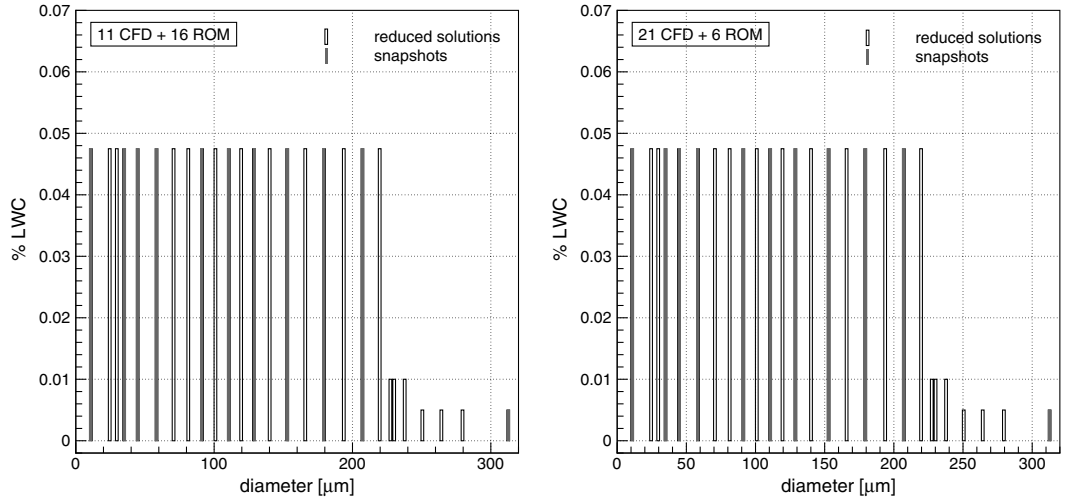

Fig. 10 Snapshots for the ice-contaminated NACA23012 at 111 μm: 11-solution set (left) and 21-solution set (right).

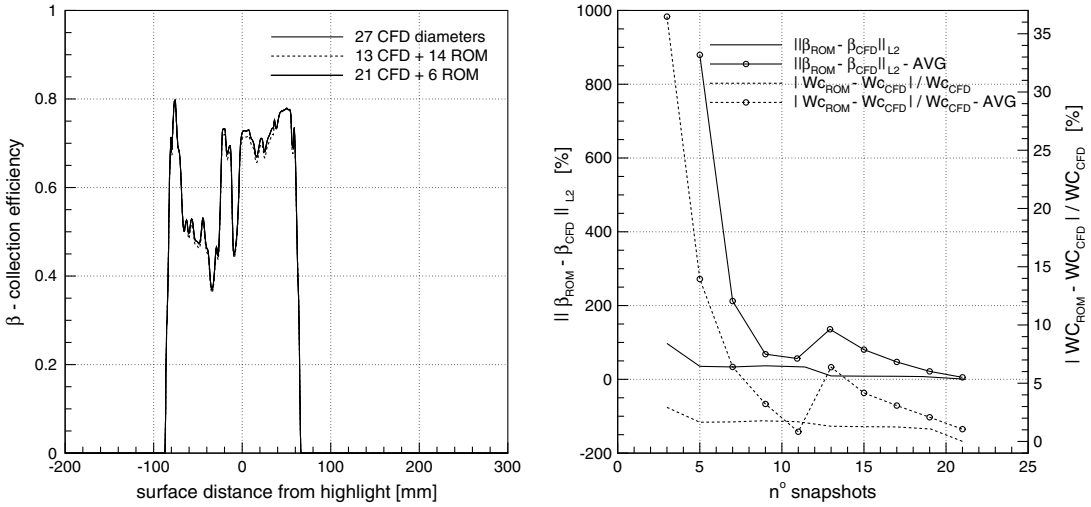

Fig. 11 MVD = 236 μm: Collection efficiency (left) and error convergence with regard to full-order 27-diameter solution, WC = water catch, kg/s (right).

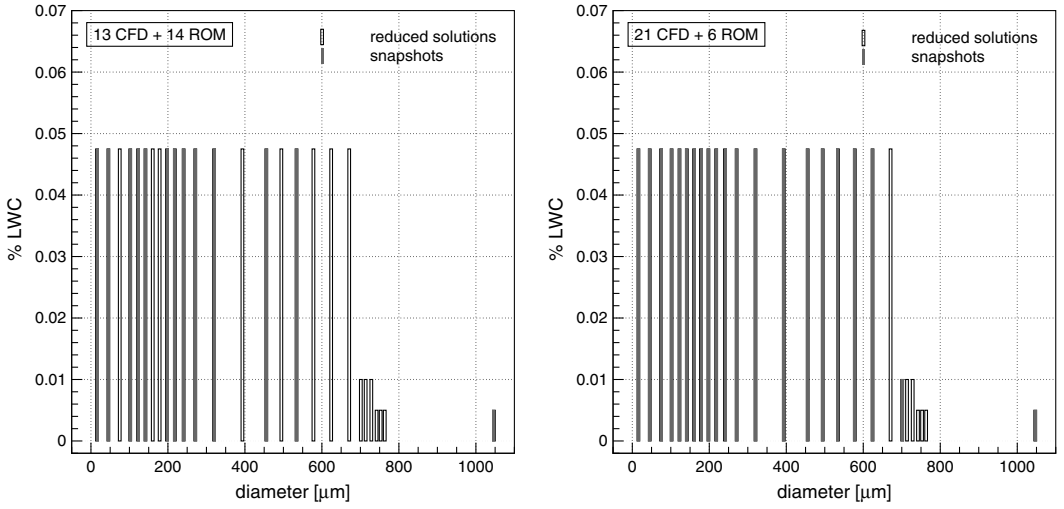

Fig. 12 Snapshots for the ice-contaminated NACA23012 at 236 μm: 13-solution set (left) and 21-solution set (right).

Fig. 13 shows the resulting local collection efficiency, β, over the aircraft surfaces computed with the 27 full-order DROP3D solutions. The highest values of β appear near the nose and the windshield, as well as on the leading edge of the nacelle inlet and the leading edge of the wing segment between the fuselage and the nacelle. Figure 13 presents the error convergence curves in terms of β and water catch for the mixed CFD-ROM and the snapshots-only cases. A minimum of 12 snapshots is required to obtain an L_2 norm of the error smaller than 10%. The error in terms of water catch is always below this threshold even in the case when only three snapshots have been adopted for the computation. The 19-snapshot solution provides an error in β smaller than 1%. Figure 14 shows the two set of snapshots with which these results have been obtained. The convergence of the 12-snapshots ROM in terms of β is 9.18%, and the error in water catch is 0.039%. In this case, the solution of the reduced model requires slightly more time, i.e., around 40 s on a single CPU, and the savings in computational time is around 60%.

To evaluate in detail the performance of the ROM approach in this case, two spanwise sections along the wing and at different locations on the nacelle have been considered. Figure 15 shows the location of these cuts. Figures 16–18 show the comparison of the extracted profiles of collection efficiency obtained, respectively, with the 27-diameter and the 12-snapshot distributions. The visual agreement is excellent, hence the inclusion of the 19-snapshot solutions that guarantees an error lower than 1% is not reported.

IX. Conclusions

In this paper, a ROM approach based on POD with the ordinary kriging interpolation technique has been applied to SLD collection efficiency in 2-D and 3-D with the aim of reducing computational

Table 2 Twenty-seven-diameter pseudo-Langmuir distributions for the DLRF6 test case

Bin	MVD = 236 μm	% LWC	Bin	MVD = 236 μm	% LWC
1	16.25	1.23	15	455.54	5.76
2	45.34	1.95	16	494.62	5.15
3	74.84	2.81	17	534.11	4.49
4	102.04	3.76	18	577.96	3.75
5	122.55	4.51	19	624.24	2.89
6	141.63	5.11	20	670.92	1.86
7	160.54	5.64	21	701.15	1.07
8	178.45	6.09	22	713.63	0.78
9	197.69	6.51	23	728.34	0.51
10	217.96	6.88	24	742.11	0.31
11	240.80	7.20	25	752.68	0.19
12	271.02	7.42	26	763.25	0.12
13	320.03	7.26	27	1046.77	0.11
14	393.53	6.58			

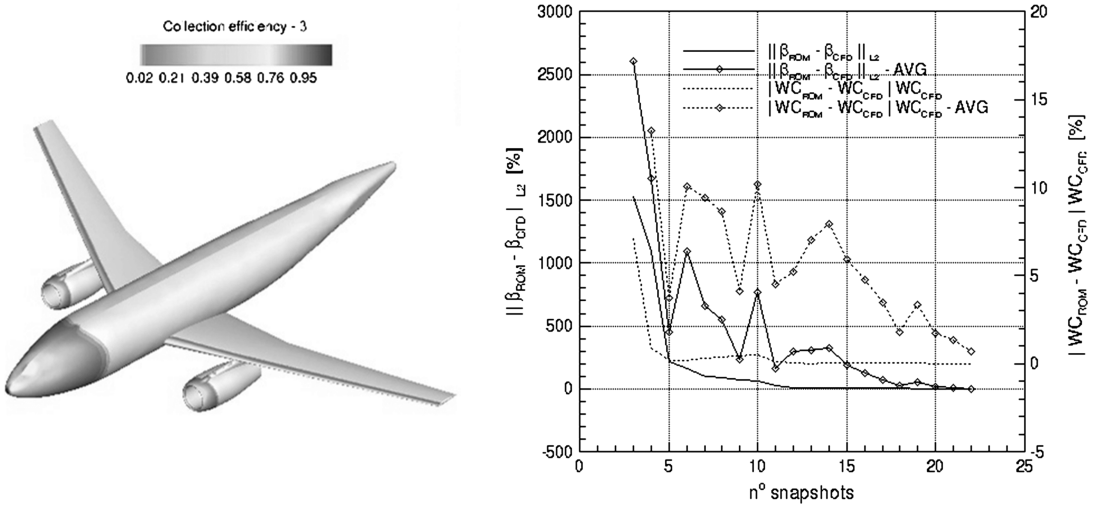

Fig. 13 Contours of local impingement efficiency β: 236 μm(left) and convergence with regard to the 27-diameter solution, WC = water catch, kg/s (right).

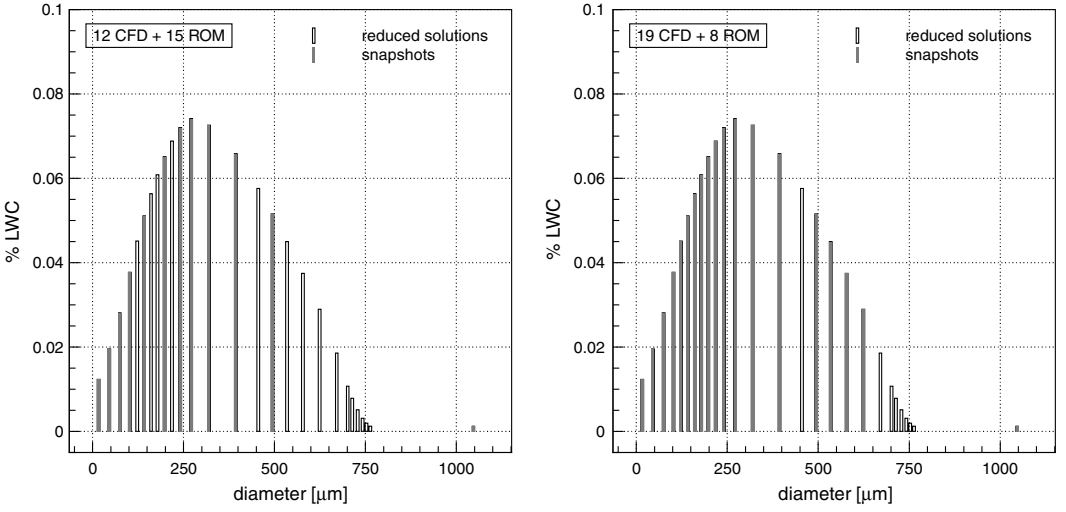

Fig. 14 Snapshots for the DLRF6 at 236: 12-solutions set (left) and 19-solutions set (right).

cost without compromising accuracy. The results show that the ROM approach is in excellent agreement with the full-order CFD solutions at a fraction of the cost. The application of this methodology to complex 3-D problems, such as impingement over an aircraft, could provide a valuable tool for the new icing certification guidelines for the SLD regime. Future research may include an evaluation of alternative techniques to extract dominant features of the flow, the selection of methods to compute the reduced-order solution, the identification of the best techniques to efficiently handle multi-parameter analyses, and, last but not least, the definition of a

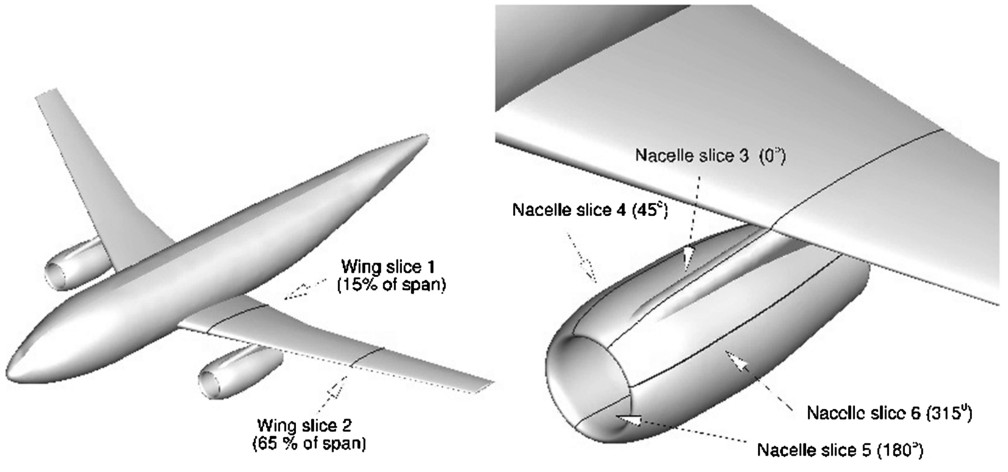

Fig. 15 Location of the slices for the β profiles extraction.

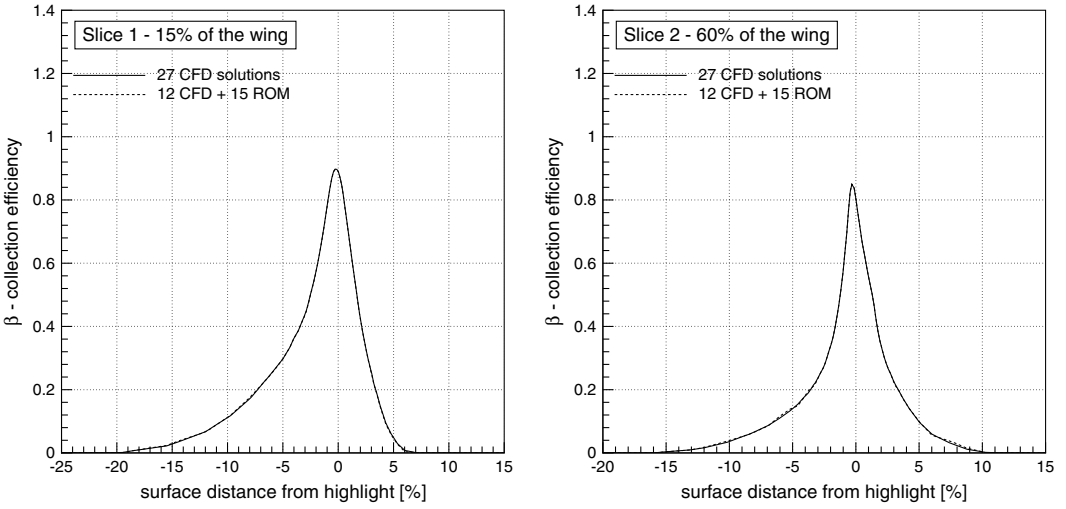

Fig. 16 Comparison of collection efficiency for DLR-F6. Wing slice 1 (left) and wing slice 2 (right).

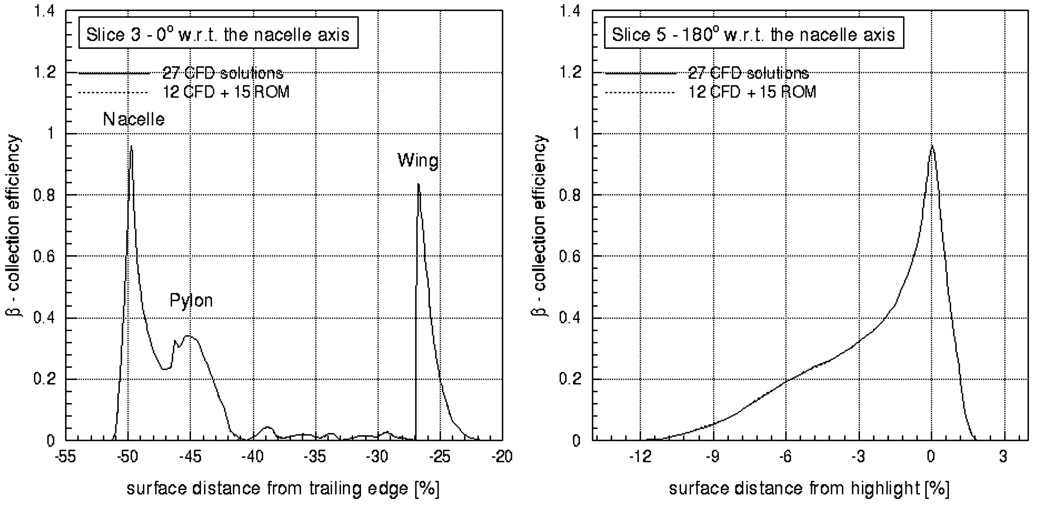

Fig. 17 Comparison of collection efficiency for DLR-F6. Nacelle slice 3 (left) and nacelle slice 5 (right).

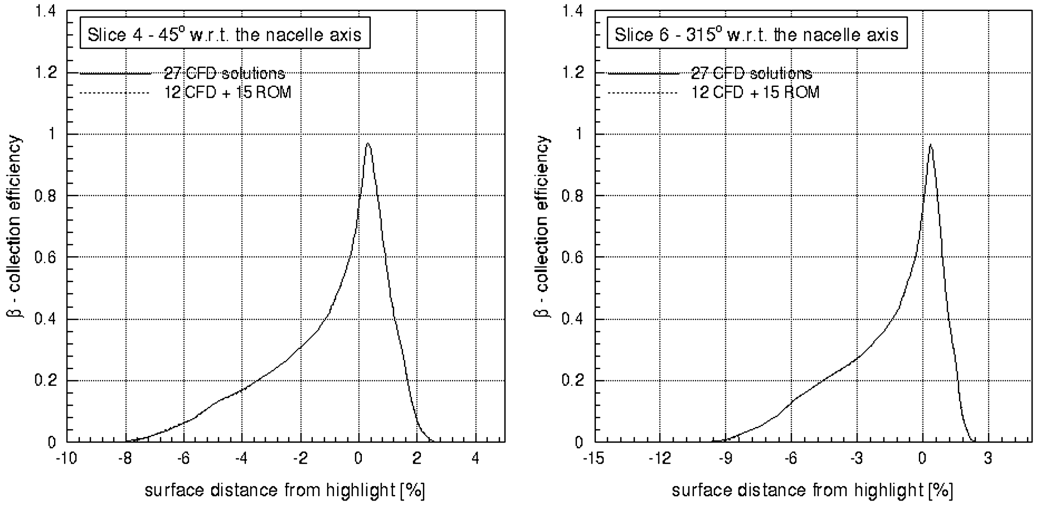

Fig. 18 Comparison of collection efficiency for DLR-F6. Nacelle slice 4 (left) and nacelle slice 6 (right).

consistent methodology that will allow the identification of the number, and most important, which particular snapshots must be selected to yield the best trade-off between computational costs and accuracy of the reduced model solutions.

Acknowledgments

The first two authors would like to thank the Natural Sciences and Engineering Research Council of Canada for financial support. We would like to thank the staff of Newmerical Technologies

International, who provided valuable guidance and comments throughout the course of this research.

References

[1] Petty, K. R., Floyd, C. D. J., "A Statistical Review of Aviation Airframe Icing Accidents in the U.S.," *Proc. of the 11th Conference on Aviation Range and Aerospace*, American Meteorological Society, Hyannis, MA, Oct. 2004.

[2] Langmuir, I., Blodgett, K. B., "A Mathematical Investigation of Water Droplet Trajectories," Army Air Forces Technical Report No. 5418, 1946.

[3] Wright, W. B., Potapczuk, M. G., "Semi-Empirical Modeling of SLD Physics," AIAA Paper 2004-0412, 2004.

[4] Schmel, R., *Advanced Modeling of Droplet Deformation and Breakup for CFD Analysis of Mixture Preparation*, ILASS-Europe 2002, Zaragoza, 9–11 Sept. 2002.

[5] Papadakis, M., Rachman, A., Wong, S., Yeong, H., Kuohsing, E., Giao, T., Bidwell, C. S., "Water Droplet Impingement on Simulated Glaze, Mixed, and Rime Ice Accretions," NASA/TM Paper 2007-213961, 2007.

[6] Papadakis, M., Rachman, A., Wong, S., Bidwell, C., Bencic, T., "An Experimental Investigation of SLD Impingement on Airfoils and Simulated Ice Shapes," SAE Technical Paper Paper 2003-01-2129, 2003.

[7] Honsek, R., Habashi, W. G., Aubé, M. S., "Eulerian Modeling of In-Flight Icing due to Supercooled Large Droplets," *Journal of Aircraft*, Vol. 45, No. 4, 2008, pp. 1290–1296.

[8] Habashi, W. G., "Recent Advances in CFD for In-Flight Icing Simulations," *Journal of Japan Society of Fluid Mechanics*, Vol. 28, No. 2, 2009, pp. 99–118.

[9] Bourgault, Y., Habashi, W. G., Dompierre, J., Baruzzi, G. S., "A Finite Element Method Study of Eulerian Droplets Impingement Models," *International Journal for Numerical Methods in Fluids*, Vol. 29, No. 4, 1999, pp. 429–449. doi:10.1002/(SICI)1097-0363(19990228)29:4<429::AID-FLD795>3.0.CO;2-F

[10] Bourgault, Y., Beaugendre, H., Habashi, W. G., "Development of a Shallow-Water Icing Model in FENSAP-ICE," *Journal of Aircraft*, Vol. 37, No. 4, 2000, pp. 640–646.

[11] Lucia, D. J., Beran, P. S., Silva, W. A., "Reduced-Order Modeling: New Approaches for Computational Physics," *Progress in Aerospace Sciences*, Vol. 40, No. 4, 2004, pp. 51–117. doi:10.1016/j.paerosci.2003.12.001

[12] Bui-Thanh, T., Damodaran, M., Willcox, K., "Proper Orthogonal Decomposition Extensions for Parametric Applications in Transonic Aerodynamics," AIAA Paper 2003-4213, 2003.

[13] Chatterjee, A., "An Introduction to the Proper Orthogonal Decomposition," *Current Science*, Vol. 78, No. 7, 2000, pp. 808–817.

[14] Everson, R., Sirovich, L., "Karhunen-Loëve Procedure for Gappy Data," *Journal of the Optical Society of America A–Optics Image Science and Vision*, Vol. 12, No. 8, 1995, pp. 1657–1664.

[15] Ly, H. V., Tran, H. T., "Modeling and Control of Physical Processes Using Proper Orthogonal Decomposition," *Mathematical and Computer Modeling*, Vol. 33, Nos. 1–3, 2001, pp. 223–236.

[16] Ravindran, S. S., "A Reduced-Order Approach for Optimal Control of Fluids Using Proper Orthogonal Decomposition," *International Journal for Numerical Methods in Fluids*, Vol. 34, No. 5, 2000, pp. 425–448. doi:10.1002/1097-0363(20001115)34:5<425::AID-FLD67>3.0.CO;2-W

[17] Fossati, M., Habashi, W. G., Baruzzi, S. G., "Impingement of Supercooled Large Droplets via Reduced Order Models," *SAE International Conference on Aircraft and Engine Icing*, SAE Paper 2011-38-0022, Chicago, IL, 2011

[18] Nakakita, K., Habashi, W. G., Nadarajah, S., "Toward Real-Time Aero-Icing Simulation Using Reduced Order Models," *Journal of Aircraft*, Vol. 47, 2010, pp. 96–109. doi:10.2514/1.44077

[19] Lappo, V., Habashi, W. G., "POD/Kriging Approximations of Multi-Disciplinary CFD Simulation with Application to In-flight Icing," *17th CFDSC Conference*, CFD Society of Canada, Ottawa, Canada, 2009.

[20] Jung, S., Myong, R., and Cho, T., "Efficient Prediction of Ice Shapes in CFD Simulation of In-flight Icing Using a POD-Based Reduced Order Model," *SAE International Conference on Aircraft and Engine Icing*, Chicago, IL, SAE Paper 2011-38-0032, 2011.

[21] Mifsud, M. J., Shaw, S. T., MacManus, D. G., "A High-Fidelity Low-Cost Aerodynamic Model Using Proper Orthogonal Decomposition," *International Journal of Bifurcation and Chaos in Applied Sciences and Engineering*, Vol. 63, No. 4, 2009.

[22] Statnikov, R. B., Matusov, J. B., "Multicriteria Optimization and Engineering," *Chapman and Hall*, New York, 1995.

[23] Iollo, A., "Remarks on the Approximation of the Euler Equations by a Low Order Model," INRIA-RR 3329, 1997.

[24] Vigo, G., "La Décomposition Orthogonale Propre Appliquée aux Équations de Navier-Stokes Compressible Instationnaire," INRIA-RR 3385, 1998.

[25] Holmes, P., Lumley, J. L., Berkooz, G., *Turbulence, Coherent Structures, Dynamical Systems and Symmetry*, Cambridge University Press, Cambridge, UK, 1996.

[26] Sirovich, L., "Turbulence and the Dynamics of Coherent Structures: 1 Coherent Structures," *Quarterly of Applied Mathematics*, Vol. 45, No. 3, 1987, pp. 561–571.

[27] Van Beers, W. C. M., Kleijnen, J. P. C., "Kriging for Interpolation in Random Simulation," *Journal of the Operational Research Society*, Vol. 54, 2003, pp. 255–262.

[28] Forrester A. I. J., Keane, A. J., "Recent Advances in Surrogate-Based Optimization," *Progress in Aerospace Sciences*, Vol. 45, Nos. 1–3, 2009, pp. 50–79. doi:10.1016/j.paerosci.2008.11.001

[29] Jeong, S., Murayama, M., Yamamoto, K., "Efficient Optimization Design Method Using Kriging Model," *Journal of Aircraft*, Vol. 42, No. 2, 2005, pp. 413.

[30] Pilch, M., Erdman, C. A., "Use of Breakup Time Data and Velocity History Data to Predict the Maximum Size of Stable Fragments for Acceleration-induced Breakup of a Liquid Drop," *International Journal on Multiphase Flow*, Vol. 13, No. 6, 1987, pp. 741–757.

[31] Trujillo, M. F., Mathews, W. S., Lee, C. F., Peters, J. E., "Modeling and Experiment of Impingement and Atomization of a Liquid Spray on a Wall," *International Journal of Engine Research*, Vol. 1, No. 1, 2000, pp. 87–105.

[32] Fossati, M., Guardone, A., Vigevano, L., "A Finite Element/Finite Volume Mesh Adaptation Technique for Compressible Flows," AIAA Paper 2010-4438, 2010.